A numerical and experimental investigation of delamination behaviour in the DCB specimen

Joakim Schön, Tonny Nyman, Anders Blom, Hans Ansell

Cet article est en exemple du type de travail qui peut être mené pour mieux comprendre, quantifier et modéliser le délaminage des matériaux composites stratifiés. Il comporte à la fois une partie expérimentale et une partie modélisation. C'est un article qui vous paraîtra compliqué en début de projet, c'est normal ne vous inquiétez pas. En fin de projet, si vous le relisez, vous devriez pouvoir le comprendre un peu mieux. Par conséquent il ne vous est pas demandé de le comprendre en détail mais seulement d'en comprendre les grandes lignes. Le travail qui vous sera demandé au cours du projet suivra les même grandes lignes. Par ailleurs, les quelques questions qui vont suivre devraient vous permettre de vous guider dans cette première lecture.

Avant d'entamer le travail, il est nécessaire de préciser quelques notions et points de vocabulaire.

- **Energy release rate** : noté G et appelé "taux de restitution de l'énergie". C'est une notion fondamentale en mécanique de la rupture qui est rapidement décrite dans la fiche projet. Nous verrons dès les premières séances que cette quantité mécanique permet de prédire dans certaines circonstances quand une fissure avance et, le cas échéant, si elle avance de manière stable ou instable. Elle est associée à une grandeur matériau appelée taux de restitution de l'énergie critique, notée G_c (on parle également de ténacité du matériau (*toughness*). Cela correspond grosso modo à une énergie par unité de surface (énergie nécessaire pour créer une fissure, c'est à fire une nouvelle surface à l'intérieur d'un milieu continu). C'est cette propriété du matériau que les auteurs cherchent à déterminer.
- **Composite laminate** : les composites qui nous intéressent ici sont dits "stratifiés", ils sont constitués d'empilements (*lay-up*) de plis (*ply*) unidirectionnels (UD). Ces plis sont de fines couches de composite. Chacune des couches est constituée de fibres de carbone alignées dans une seule direction. On les empile en faisant varier les directions (0°, 45°, 90°, etc) (*stacking sequence*).
- dénomination d'un composite : on les désigne souvent par le couple fibre/matrice. Ainsi le T300/914 est constitué de fibres T300 (dénomination commerciale) et d'une matrice époxy 914 (dénomination commerciale).
- nomenclature d'un stratifié : on note les angles des plis successifs entre crochets. Ainsi [0/90/45/45/90/0] désigne un stratifié de 6 plis orientés suivant la séquence indiquée. Quand la stratification est symétrique, on peut n'en écrire que la moitié et mettre un indice $_S$. Le stratifié précédent s'écrit donc également $[0/90/45]_S$. Quand plusieurs plis adjacents ont la même orientation, on note leur nombre en indice. Ainsi un [45/45/0/0/0] s'écrit également $[45_2/0_3]$
- **FEM ou FE** : signifie *Finite Element Method* ou *Finite Elements*.

Voici quelques questions destinées à vous guider dans la lecture de l'article.

section 1 : Introduction

— quels sont les critères dimensionnants d'une structure composite aéronautique ?
— à cause de quoi peuvent apparaître les délaminage ?
— quels sont les deux grands types de sollicitations considérés dans cet article ?
— quel type d'essais sera mis en œuvre et analysé ?

section 2 : Numerical and experimental procedure

— section 2.1 : les auteurs veulent étudier le délaminage entre deux plis orientés de la même façon mais pour trois angles différents par rapport au repère global de sollicitation de l'éprouvette : 0°/0°, 45°/45°, 90°/90°. Comment procèdent-il pour faire ces trois types d'essais ?
— section 2.3 : Les quantités E_{11}, E_{22} et E_{33} sont des modules d'Young (du modèle élastique). Pourquoi y en a-t-il 3 et pas 1 seul comment habituellement ?
— section 2.4 : quelles sont les trois quantités mesurées pendant l'essai ?
— section 2.4 : l'expression (1) donne une valeur de taux de restitution de l'énergie. En cours de projet, vous serez amené à démontrer cette expression. Mais pour l'instant, retrouvez vous les 3 quantités dont il était question dans la question précédente ?

section 3 : Experimental results

— pourquoi les auteurs attendent-il 20 à 30s avant de faire leurs mesures ?
— figure 4 : à quoi correspond la chute d'effort sur les relevés expérimentaux ?
— figures 6 et 7 : les auteurs relèvent les G_c (taux de restitution de l'énergie critique) en fonction de la longueur de fissure mesurée pour les interfaces 45/45 et 90/90. On appelle ces courbes des courbes de résistance (ou courbe R). Peut-on dire que le G_c mesuré est dans ce cas une grandeur intrinsèque du matériaux ?
— Les auteurs ne montrent pas la courbe obtenue pour les interfaces 0/0, mais ils décrivent ce qu'ils observent. À quoi ressemblerait la courbe R pour une interface 0/0 ?
— Quel est le meilleur matériau vis a vis du délaminage parmi les 3 testés ?
— section 3.2 : les auteurs réalisent des observations par microscope sur certaines éprouvettes cassées. Quelle est la grande différence entre les fissures des interfaces 0/0 d'une part et les fissures des 45/45 et 90/90 d'autre part ?

section 4 : numerical results

— Les auteurs réalisent un calcul 3D. Ils constatent que le G n'est pas constant le long du front de fissure. Comment expliquent-ils cela ? Notamment au regard du faciès de rupture de la figure 10.
— Les figures 14 et 15 présentent l'évolution de la souplesse des éprouvettes (*compliance*) en fonction de la longueur de fissure, elles comparent notamment la mesure expérimentale à la prédiction par éléments finis (STRIPE est leur logiciel éléments finis). La figure 15 apporte une correction du modèle, en quoi consiste-elle ?

section 5 : Implication for aircraft design

— Quel est le G_c apparent le plus faible entre une sollicitation monotone (statique) et une sollicitation en fatigue ?

ELSEVIER

Composites Science and Technology 60 (2000) 173–184

COMPOSITES SCIENCE AND TECHNOLOGY

A numerical and experimental investigation of delamination behaviour in the DCB specimen

Joakim Schön [a], Tonny Nyman [b,c,*,1], Anders Blom [a,c], Hans Ansell [b]

[a] *The Aeronautical Research Institute of Sweden, PO Box 1102 1, S-16111 Bromma, Sweden*
[b] *Saab AB, S-58188 Linköping Sweden*
[c] *The Royal Institute of Technology, S-10044 Stockholm, Sweden*

Received 9 November 1998; received in revised form 8 July 1999; accepted 4 August 1999

Abstract

An extensive numerical and experimental investigation has been carried out on the fracture mechanical properties of DCB specimens. Static and cyclic properties were studied for different interfaces (0°/0°, 45°/45° and 90°/90°) and for several materials, IM7/8552, HTA7/6376 and T300/914. Different data-analysis methods have been compared and two beam models have been compared to a FE solution. Basic studies undertaken include modelling and experimental observation of delamination growth in DCB specimens. State of the art FE analyses are described and the energy release rate of the specimens is calculated. Two beam models are compared with the FE results and it is found that the more advanced beam model is more accurate. Experimental results are interpreted in terms of usefulness for applications to real structures. Toughness measurements on DCB specimens show that non-zero interfaces have a plateau value roughly four times higher than the onset value, which is almost the same as for the zero interface. Higher toughness values are probably due to the fact that the initial crack deviates from the original symmetrical crack plane. The experimental data collection methods corrected beam theory and Berry's method give similar results. Numerically predicted curved crack front for zero-interface could be verified experimentally. The delamination growth rate during fatigue increased rapidly with increasing applied energy release rate and the 0°/0° interface had the highest growth rate. The specimen with a 90°/90° interface has the flattest energy release rate distribution and the specimen with a 45°/45° interface the most uneven one. The material systems IM7/8552 and HTA7/6376 have higher critical energy release rates than T300/914.

1. Introduction

The new Swedish fighter, the Saab JAS39 Gripen utilises approximately 30 wt% of carbon fibre/epoxy composite laminates in the primary structure. Currently, the main design drivers for most composite structural components are either stiffness, static strength or low energy impact damage. In order to avoid structural problems current design procedures have led to rather low allowable strain levels. It is anticipated that these values will be increased in future aircraft and then it may be necessary to further consider the likelihood for fatigue damage. In the certification process, durability and damage tolerance criteria require composite structures containing undetected damage to be acceptable to fly. Comparing different types of damage, manufacturing or service induced, delamination growth is considered one of the most important failure mechanisms that can be detrimental for flight safety.

Consequently, delaminations must be considered not only in the design process, but also in structural verification testing. Examples are delamination growth due to local buckling, delamination growth from free edges and notches such as holes, delamination growth from ply drops, and impact damaged composites containing considerable amount of delamination. Delamination growth can occur as a consequence of interlaminar stresses which can arise from fuel pressure variations, stiffness mismatch and in complex structures due to unanticipated loading. It is important, therefore to improve the knowledge of delamination growth both theoretically and experimentally. The most straightforward way is by studying simple test specimens, such as

* Corresponding author. Fax: +46-13-183363.
E-mail address: tonny.nyman@saab.se (T. Nyman).
[1] Currently a part-time research student at the Royal Institute of Technology, Department of Aeronautics, S-10044 Stockholm, Sweden.

0266-3538/00/$ - see front matter
PII: S0266-3538(99)00113-X

the double-cantilever beam (DCB) specimen. It is also of interest in aircraft design to build up a database of material toughness on advanced carbon-fiber composites, (CFC), currently in use or considered for use in airframe structures.

It is generally believed that the mode separated energy release rate of delamination growth is a good measure of the composite materials resistance to delamination growth. Delamination growth can be separated into two different types, monotonic loading, e.g. due to very large accidental overloading, and fatigue loading. By using the DCB specimen the critical mode I energy release rate, G_{Ic}, can be measured and this information, combined with critical mode II and mode III energy release rate data, G_{IIc} and G_{IIIc}, can then be used for comparing different composite materials and to increase the understanding of delamination growth in composite materials.

Several round-robin tests of unidirectional composites have been performed, with focus on e.g. delamination onset, T tab vs hinge, insert type and thickness [1]. A matter of concern has also been where to evaluate G_{Ic}; onset of nonlinearity; at the load corresponding to 5% offset in initial compliance or at the load at visual observation of delamination onset at the edge.

In order to obtain consistent results when analysing experimental data it is necessary to consider deflection of the crack tip, the effective shortening of the beam as a result of large displacements and end-rotation of the arms, but also the stiffening of the beam caused by the presence of the blocks bonded to the specimens [2]. The simple beam theory has difficulties simulating the deformation near the crack tip. More advanced models have been introduced by Olsson [3], and Sun and Pandey [4]. In comparison to a finite-element solution the FE results lie between the results obtained from the Olsson, and Sun and Pandey models [5].

The energy release rate along a straight crack will not be constant, but approaches zero or infinity, depending on interface ply orientation at the vertices, where the crack intersects the free surface. This will cause the crack to become curved and the angle the crack makes with the surface is determined by the interface ply orientation [6]. A ratio $D_C = D_{12}^2/(D_{11}\ D_{22})$ has been introduced [7,8], and was found to correlate with the difference in energy release rate at a specimen's centre versus that at its edges [8]. A stiffness ratio $B_t = D_{16}/D_{11}$ has been introduced and was found to correlate with the asymmetry in the energy release rate distribution about the centre of the specimen's width [7,8]. Since the energy release rate is not evenly distributed along a straight crack the crack tip will become curved. This has been studied analytically [7,9] and by FE computations [10].

The crack initiation has been studied by microfocus radiography and it was found that the crack initiates in the interior of the specimen, resulting in a curved crack tip, and that the crack initiation corresponds to the non-linear load/displacement curve [11]. For carbon-fibre/epoxy composite specimens the interfacial ply orientation does not have a significant effect on G_{Ic} values [12,13]. An overview of experiments and analyses being performed at the coupon level within the GARTEUR (Group of Aeronautical Research and Technology in Europe) action group AG 16 can be found in Ref. [14].

To provide a basis for development of a structural analysis capability there is a need for property data obtained from coupon testing. Such data could provide a basis upon which residual strength and delamination growth prediction methods might be based.

The objective of the present investigation was to develop a fracture mechanics approach to assess the damage tolerance of composite materials. The G_{Ic} value of three material systems should be compared. Three interfaces, 0°/0°, 90°/90° and 45°/45° should be studied and the results should be related to fractographic investigations. The delamination growth during fatigue loading should be measured for the different interfaces. The energy release rate of test specimens should be calculated with 3D FEM and the results compared to different beam models.

2. Numerical and experimental procedure

2.1. Geometry

Baseline material for the testing was IM7/8552 for which different interfaces were investigated. In order to compare the materials HTA7/6376 and T300/914 with IM7/8552, specimens with 0°/0° interfaces were used. Specimens were prepared from graphite/epoxy prepreg of IM7/8552, HTA7/6376 and T300/914, and were processed into 24 layer thick plates, approximately 3.12 mm thick. The starter delaminations, inserts, were produced using a fluorinated polymer release film, 10 μm thick between central plies. The plates were cut into specimens with the geometry given in Fig. 1 and piano hinges

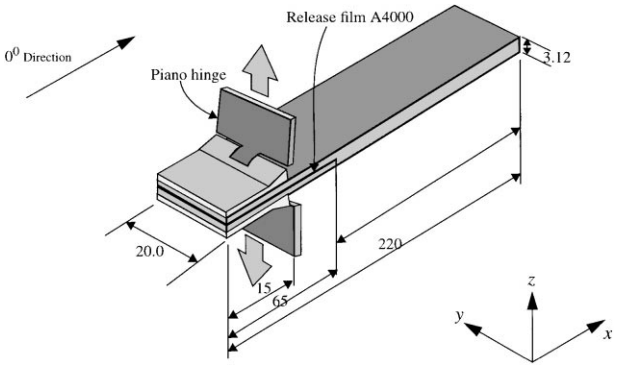

Fig. 1. Schematic illustration of DCB specimen used for testing.

were adhesively fastened to the specimen in order to aid the application of a crack opening force. Stacking sequences used are shown in Table 1. The reasons for choosing these stacking sequences were that, at the time for the experimental investigation, considerable time was devoted to 0°/0° interfaces and very little was done for other interfaces reflecting more realistic layups.

The starter crack was located at the centre of the specimens which resulted in 0°/0°, 90°/90° and 45°/45° interface cracks. The layups used resulted in both the cracked and uncracked part of the specimen having a symmetrical layup which reduces the residual thermal stresses and unnecessary bending-twisting coupling.

2.2. Numerical procedure

The numerical modelling was performed with an in-house developed finite element program, STRIPE, which is based on an hp version of the finite element method [15]. The program increases the polynomial order (p-value) of the elements which results in a series of solutions, where each solution is for a different p-value. Since the convergence properties of the solution is known [6], it is possible to determine when a satisfactory convergence of the solution has been reached by comparing the solutions for different p-values.

2.2.1. Mesh design

The specimens were modelled with 3-dimensional solid brick elements and each ply layer had one element in the thickness direction. Six elements were placed along the crack tip with the length of the elements increasing a factor 6 in the y-direction, starting from the edges of the specimen. This was done in order to handle the vertex singularity which occurs where the crack tip intersects the free surface [6]. The elements also increased by a factor of 6 in length in the x-direction when going away from the delamination front. Inside the elements which are next to the crack tip 5 layers of elements were created with their length, going away from the crack tip, increasing by a factor of 6.6 between each layer. The hinges, where the force was applied, were modelled as 1 mm thick steel layers with the force applied as a uniform pressure over a 1×20 mm area. A schematic of the mesh can be seen in Fig. 2 where the location of the crack is enlarged in the lower part of the figure.

2.3. Material

2.3.1. Basic material data

Material data used in calculation are for IM7/8552 given in Table 2, room temperature data, where the subscript 11 stands for the fiber direction, 22 is perpendicular to the fiber direction, but in the plane of the ply, and 33 is the direction perpendicular to the plane of the ply.

2.4. Testing procedure

The testing was undertaken in accordance with the ESIS-protocol [16]. All testing was done at room temperature with dry laminates, RTD, and under displacement control. Prior to testing, the edges of the DCB specimens were painted with typewriter correction fluid to assist visual crack length determination with a travelling microscope. Load displacement curves were recorded during loading and un-loading. After loading, during displacement control, the crack continued to grow for a while. It was therefore decided to allow the crack to stabilize for 20–30 s before data, displacement, force and crack length, were collected.

The cyclic tests were performed at constant amplitude, $R = \delta_{\min}/\delta_{\max} = 0.1$, with a frequency of ~6.5 Hz. The displacement level chosen was initially set to a displacement corresponding to 80% of maximum load on the un-loading curve established during pre-cracking procedure, see Fig. 3.

In general, recording crack-length as a function of number of cycles requires short intervals, especially in the beginning, since the crack propagation is very fast.

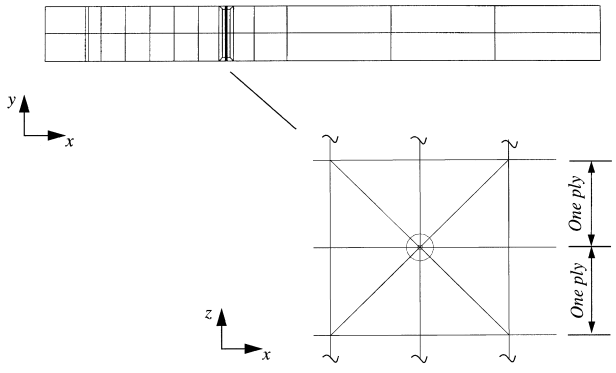

Fig. 2. Schematic illustration of the FE mesh.

Table 1
Laminate configurations

Laminate	Stacking sequence
A	$[0_{12}]_s$
B	$[90/0/90/0/90/0_2/90/0/90/0/90]_s$
C	$[45/-45/90/0/-45/45_2/-45/0/90/-45/45]_s$

Table 2
Material data for IM7/8552

$E_{11} = 160$ GPa	$E_{22} = 10$ GPa	$E_{33} = 10$ GPa
$G_{12} = 4.8$ GPa	$G_{13} = 4.8$ GPa	$G_{23} = 3.2$ GPa
$v_{12} = 0.31$	$v_{13} = 0.31$	$v_{32} = 0.52$
$t_{nom} = 0.13$ mm		

To maintain a constant R-ratio of 0.1 related to $G(R_G = G_{\mathrm{Imin}}/G_{\mathrm{Imax}})$ during testing can be difficult, since as the crack length increase and $\Delta\delta$, change in deflection, is constant the load decrease, thus causing fluctuations in R_G.

2.4.1. Data analysis methods

For analysis of the test results three different calculation methods were used to estimate toughness, simple beam theory ($G_{\mathrm{Ic}}T$), corrected beam theory ($G_{\mathrm{Ic}}CB$) and Berry′s method ($G_{\mathrm{Ic}}B$), see e.g. Refs. [16] and [17]. The simple beam theory expression assumes the DCB specimen to behave as a built-in beam. The energy release rate becomes,

$$G_{\mathrm{I}} = \frac{3P\delta}{2Wa} \tag{1}$$

where P is the applied load, δ is the crack-opening displacement at the point where the load is applied, W is the width of the specimen, and a is the crack length.

In practice, this expression will underestimate the compliance as the beam does not behave as if it is perfectly built-in. Two methods to correct for this effect are: (1) the corrected beam theory which treat the beam as containing a slightly longer crack, $a+\Delta$, where Δ may be found experimentally by plotting the cube root of compliance, $C^{1/3}$, as a function of crack length, or (2) to modify the factor of three using experimental data, i.e. the Berry method.

The energy release rate for the corrected beam theory is then given as

$$G_{\mathrm{I}} = \frac{3P\delta}{2W(a+\Delta)} \tag{2}$$

This provides a useful check on the procedure, since a value independent of crack length should be obtained.

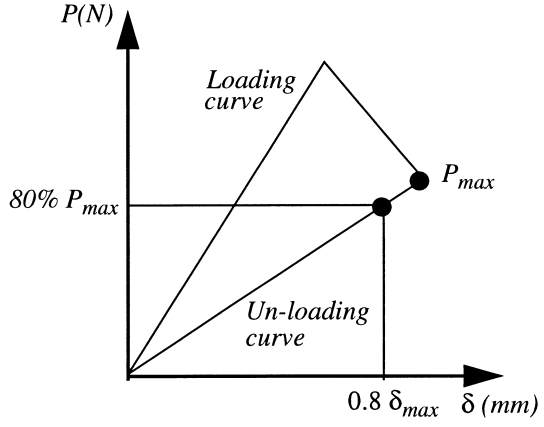

Fig. 3. Schematic illustration of the method of establishing load levels in cyclic testing.

Berry's method is to plot compliance versus crack length on a log–log plot. The slope of this plot n can then be used to give G_{I} as

$$G_{\mathrm{I}} = \frac{nP\delta}{2Wa} \tag{3}$$

3. Experimental results

3.1. Static

3.1.1. Zero-interface

A typical load-displacement curve for a zero-degree interface is shown in Fig. 4. Two different curves are shown, one where the load was measured immediately after loading (displacement control) and one curve where the crack was allowed to stabilize before measurement, which required approximately 20–30 s. The initial drop in load as the crack advanced from the insert was typical for all tests. The influence of the starter crack can be seen within the circle.

Evaluation of toughness using Berry′s method and the corrected beam method leads to similar results, typically lower than by the simple beam theory. The longitudinal modulus E_f was calculated according to the corrected beam method, which typically resulted in an error less than 5% when compared to the expected longitudinal modulus, see Table 2. No toughness increase with crack length, after initial settlement, was observed for the 0°/0° interface. The average G_{Ic} values, analysed with Berry's method, for the three material systems, IM7/8552, HTA7/6376, and T300/914 are $220 \pm 10, 230 \pm 3$ and 112 ± 10 N/m, respectively. The HTA7/6376 material system has a slightly higher G_{Ic} value than the IM7/8552

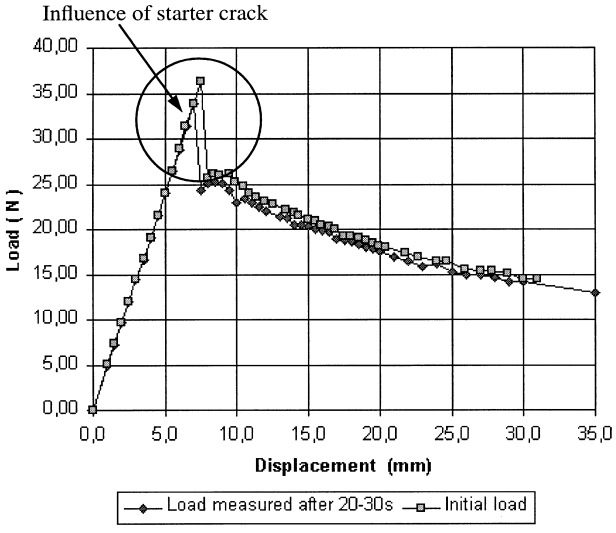

Fig. 4. Load/displacement curve for a typical zero interface, IM7/8552.

material system, 5%, but the difference is within the 95% error bounds. The T300/914 material system has a G_{Ic} value which is only half that of the other two material systems. This demonstrates the improvement in toughness of the more modern material systems IM7/8552 and HTA7/6376 when compared to the older material system T300/914, see Fig. 5.

3.1.2. Non-zero interface (45°/45° and 90°/90°)

For non-zero interfaces a toughening curve was observed, see Figs. 6 and 7, After initiation, which occurred at a similar G_{Ic} value as for the 0°/0° interface, G_{Ic} increased rapidly. After approximately 10 mm crack propagation G_{Ic} had reached a plateau value for the specimens with a 90°/90° interface. In the plateau region the crack propagation was characterized by crack arrests and propagation. The specimens with a 45°/45° interface showed a similar toughening behaviour with the major difference being that the crack had to propagate approximately 15–20 mm before the plateau region was reached. The pre-cracking toughness for the 90°/90° and 45°/45° interfaces were 335 ± 30 and 180 ± 60 N/m, respectively. Although, the error bounds are large there appears to be a fiber direction dependence on the G_{Ic} especially on the plateau value, which is, approximately 20% larger for the 90°/90° interface than for the 45°/45° interface.

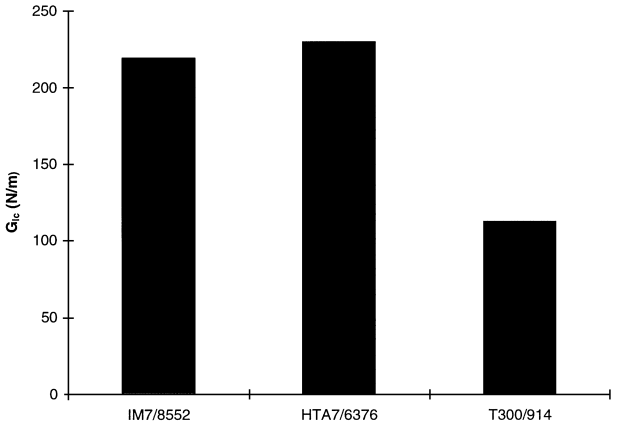

Fig. 5. Mode I toughness testing. Comparision between different UD materials.

3.2. Fractographic investigation

A fractographic investigation was undertaken on some of the specimens [18]. Four specimens were examined, one HTA7/6376 with 0°/0° interface and three IM7/8552 with 0°/0°, 45°/45° and 90°/90° interfaces. Both specimens with a 0°/0° interface have smooth fracture surfaces which are dominated by matrix failure. The smooth crack surfaces explains why no toughening behaviour was observed.

The specimen with the 90°/90° interface showed a rough fracture surface with the crack propagating within the 90° ply, being bounded by the surrounding 0° plies, see Fig. 8a. The crack propagation direction is from left to right in the figure. When crack propagation begun it propagated directly from the insert to one of the 0°/90° interfaces and it propagates only in the matrix breaking only few fibres. If the crack should propagate into the 0° ply it would have to break the fibres. But, it is easier for the crack to follow the interface. Therefore, it is not able to propagate into the 0° plies. It then changed 0°/90° interface in a periodic fashion. When the crack changed interface the crack propagated at approximately 45° angle to the global crack-propagation direction. When the delamination crack changes interface it is similar to a matrix crack. This type of behaviour has been observed earlier by Wilkins et al. [19], and Chai [20]. A possible explanation for this type of crack growth, based on directional stability considerations, has been given by Chai [20]. It is probable that the wavy crack path is the cause of the observed toughening behaviour. Since the plateau region was reached after approximately 10 mm, it can be expected that approximately 10 mm of crack surface

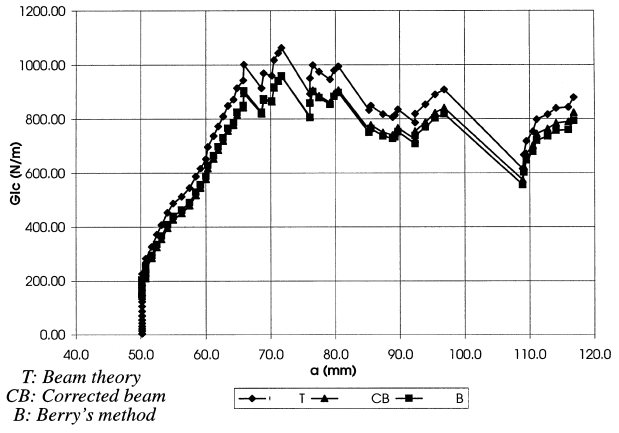

Fig. 6. A typical R curve from a 45° interface, IM7/8552 material.

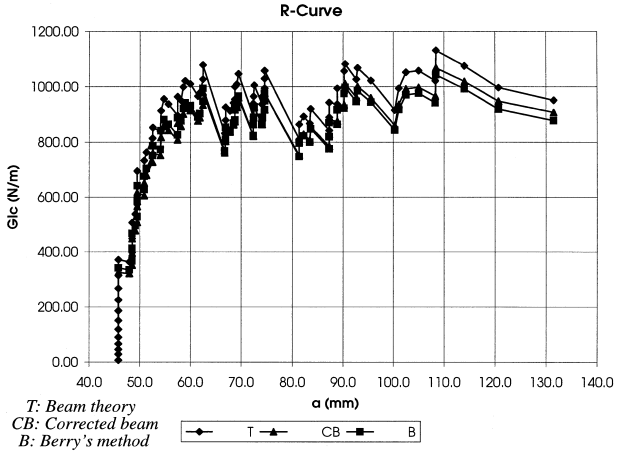

Fig. 7. A typical R curve from a 90° interface, IM7/8552 material.

behind the crack tip is involved in the toughening. Fig. 8b is a more detailed view of the crack surface normal to the global crack direction. The crack propagation direction is from the top to the bottom in the micrograph. In the top and bottom of the micrograph the crack has propagated from one 0°/90° interface to the other. In the middle part of the micrograph the crack has propagated at the 0°90° interface. When the crack has propagated through the matrix it reaches the 0°/90° interface which it then follows. As the crack propagates further at the 0°/90° interface the interest to change interface again increases as the crack length increases. This can be seen in the micrograph where marks from the 0° fibres are clearly visible just as the crack has reached the 0°/90° interface. This suggests that the crack would like to propagate into the 0° fibres, but it can not break them. Instead it follows the interface of the fibres closely. As the cracks advance further the marks from the 0° fibres vanish. Instead, some 90° fibres are becoming visible. This suggests that the crack would more and more like to change interface again. Close to where the crack changes interface several 'matrix cracks' are visible. Most of the matrix cracks reaches one of the free edges of the specimen. But, some matrix cracks both start and ends inside the specimen. This suggests that several matrix cracks nucleate in the interior of the specimen and maybe at the edges when the delamination crack tries to change 0°/90° interface. The observation that matrix cracks end inside the specimen would suggest that they propagate parallel to the 90° fibres, y-direction, after having nucleated through the two 90° plies. Fig. 9 shows the surface of a matrix crack between the two 0°/90° interfaces. The crack has globally propagated from the top to the bottom in the micrograph. But, locally it has probably propagated parallel to the 90° fibres. This probably results in a mode II component being introduced locally which results in hackles being formed, see Fig. 9. Those hackles have the highest concentration in the middle between the two 0°/90° interfaces and the lowest concentration close to the 0°/90° interfaces. Several matrix cracks are visible close to where the delamination crack changes interface. But, the delamination crack does not change interface until one of them have propagated through the total width of the specimen. In Fig. 7 it can be seen how the crack has propagated and then arrested. The points where it has arrested might be when it was nucleating matrix cracks and waited for one of the matrix cracks to propagate through the total width of the specimen. It probably requires a high applied force to make the matrix cracks propagate in the y-direction when the global crack direction is in the x-direction. This might be one toughening mechanism behind the *R*-curve behaviour. Since not all the fibres in the 90° plies are perfectly parallel the matrix crack has to break some fibres when propagating through the width of the specimen,

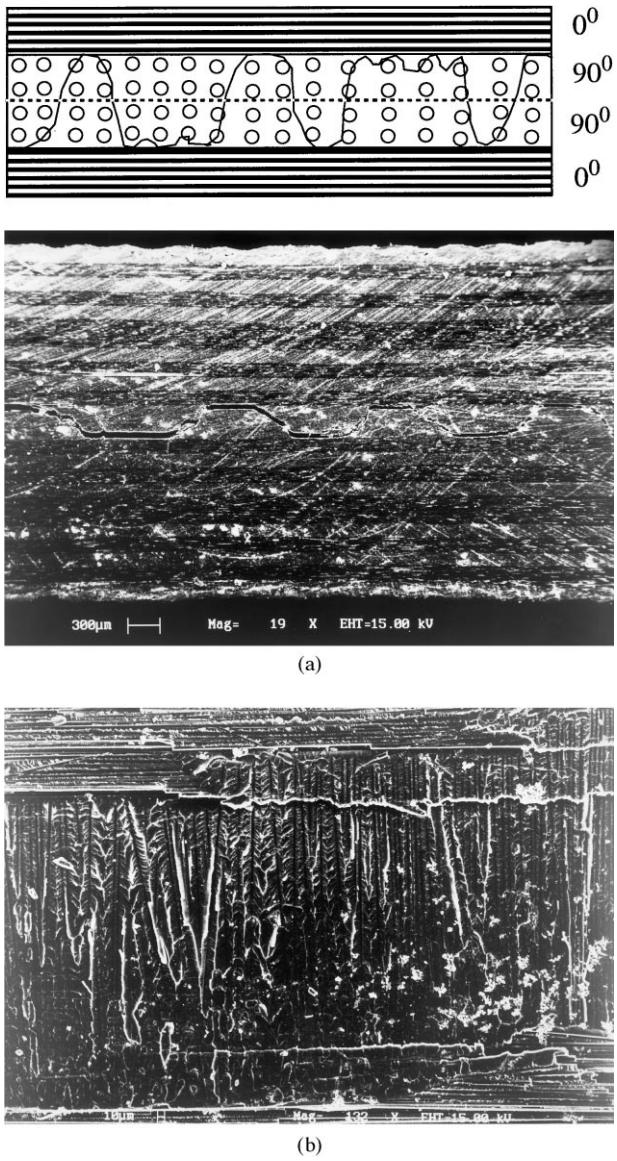

Fig. 8. Crack growth at 90°/90° interface between two adjacent 0° plies.

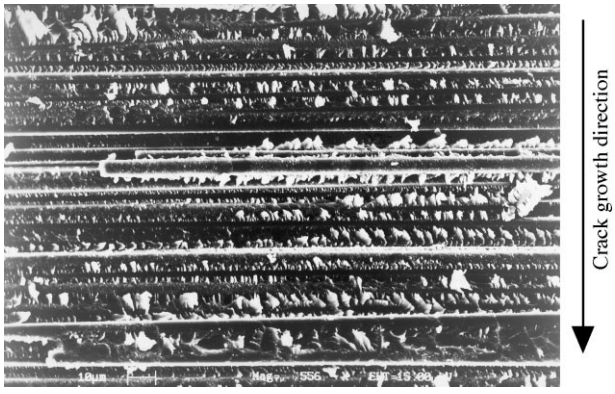

Fig. 9. Hackles conforming a mode II shear fracture [18] in a specimen at 90°/90° interface.

see Fig. 9. This might be another toughening mechanism. The matrix cracks could also have been caused by the tensile flexure stresses ahead of the crack tip. The delamination would then have joined the matrix cracks together. If the matrix cracks would have formed ahead of the crack tip they would have been evenly distributed. But, since matrix cracks are only observed where the delamination crack changes interface this is not probable, see Fig. 8.

A similar behaviour was observed for the specimen with the 45°/45° interface as the delamination propagates from the insert with the difference that the "ridges" were parallel to the 45° fibres. Another difference from the 90°/90° specimens is the distance the crack has to propagate before the plateau value is reached. Since the crack originates between 45° plies and the crack can not break fibres, the crack will change interface at one side of the specimen. The change of interface will then "propagate" into the specimen at an angle of 45°. This causes a large part of the crack surface to be initially smooth. The fracture toughening is not fully developed until the change of interface has extended over the total width of the specimen. This requires the crack to propagate 20 mm, i.e. the same length as the specimen is wide, and this was consistent for all specimens with that type of interface. This explains why the crack propagation distance before the plateau value is reached is larger for the 45°/45° interface than for the 90°/90° interface, see Figs. 6 and 7. Since the fibres are in the 45° direction and the crack tip is approximately in the 90° direction, the crack tip will shift interface several times over the total width of the specimen. When the crack has propagated out of the centre plane of the specimen 'globally' a small modus II component is introduced. It is believed this component is sufficiently small to be neglected. But, it should be pointed out that the beam models only reflect the 'global' behaviour. The local details when the crack changes interface is not included.

Also confirmed is the curved crack front for a DCB specimen, HTA7/6376, with 0°/0° interface, see Fig 10. For other interfaces it was not possible to determine the shape of the crack front.

3.3. Fatigue experiments

Specimens with 0°/0° interface had the lowest resistance to delamination growth in fatigue, followed by specimens with 45°/45° interface while specimens with 90°/90° interface had the highest resistance, see Fig. 11, where the data have been analysed with the simple beam theory, Eq. (1). Considering the toughening behaviour observed for 45°/45° and 90°/90° interfaces it is not surprising that those interfaces have a higher resistance to delamination growth than the 0°/0° interface. In Fig. 12 a comparison is made between IM7/8552 and HTA7/6376 with 0°/0° interface. The slopes are very high indicating that it is almost impossible to take advantage of stable delamination growth in carbon/epoxy material loaded in modus I. To differentiate between the two materials is also almost impossible. The crack growth rate is assumed to follow Paris law,

$$\frac{da}{dN} = S(\Delta G)^m \tag{4}$$

where S and m are constants. In this case m is approximately 16 which is an order of magnitude larger than for metals. In Table 3, published m-values for different materials can be seen as a comparison. The measured m-value is above average, but not the highest reported value.

No threshold value for delamination growth was observed from the data. However, if the results are extrapolated to a delamination growth rate of $1{\cdot}10^{-6}$ mm/cycle a threshold value for practical applications can be considered to have been reached.

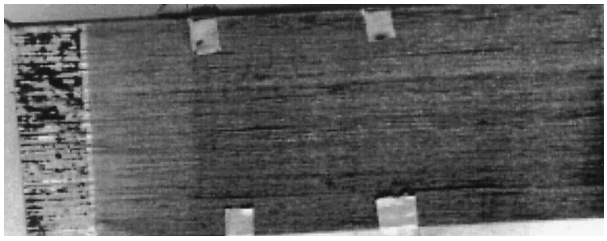

Fig. 10. Curved crack front shape for a DCB specimen with zero interface, HTA7/6376. The crack propagated from left to right.

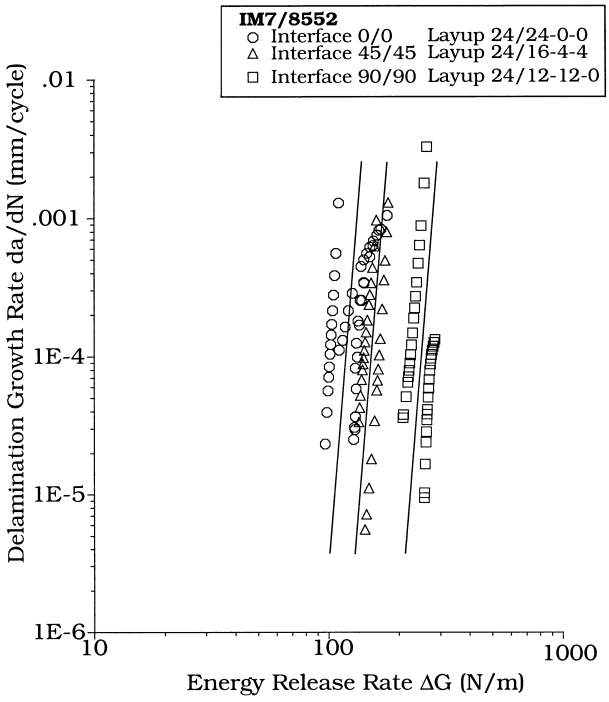

Fig. 11. Delamination growth rate as function of energy release rate ΔG for DCB specimen, different interfaces considered.

4. Numerical results

4.1. Convergence

The convergence of the numerically calculated energy release rate was studied by increasing the polynomial degree of the elements, *p*-value. The obtained peak and average energy release rates along the crack tip for the different layups can be seen in Tables 4 and 5. The data are for specimens with 50 mm crack length and an applied force P of 100 N. For the 0°/0° interface a satisfactory convergence had been reached for a *p*-value of 4 and for the 90°/90° and 45°/45° interfaces a *p*-value of 5 was required, see Table 4.

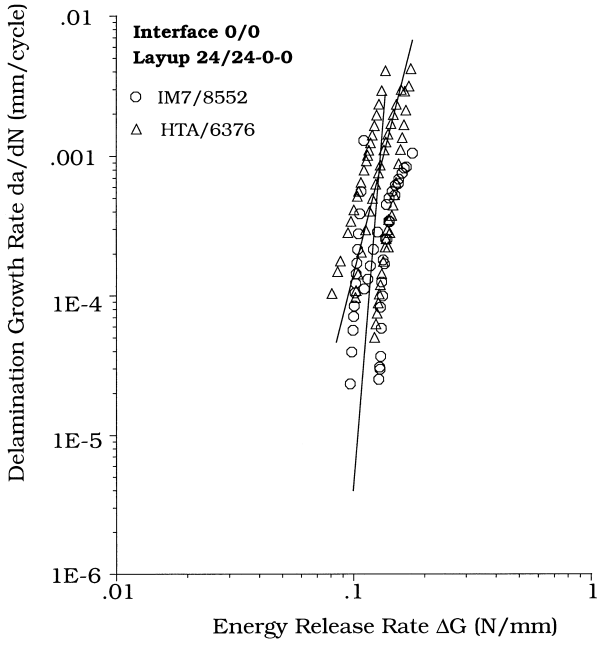

Fig. 12. Delamination growth rate as function of energy rate ΔG for DCB specimen, different materials considered.

Table 3
Published *m*-values for different materials and *R*-value

Material	*R*-value	Mode	*m*	Reference
T300/914C	0.1	G_I	10.6	[23]
T300/914	0.1	G_I	7.0	[24]
T300/914	0.2	G_I	7.5	[24]
T300/914	0.3	G_I	7.0	[24]
T300/914	0.5	G_I	8.0	[24]
T300/‡2500	0.2	G_I	9.0	[24]
T300‡2500	0.5	G_I	12.5	[24]
T300‡2500	0.7	G_I	21.5	[24]
M40/Code69	0.1	G_I	28	[23]
AS4/PEEK	0.5	G_I	6	[23]
AS4/PEEK	0.2	G_I	5	[23]
AS4/PEEK	0.1	G_I	6.1	[25]
AS4/PEEK	0.5	G_I	8.5	[25]

4.2. Distribution of G along crack front for different layups

The distribution of energy release rate along the crack tip for a straight crack can be seen in Fig. 13. The data are for the analysed specimens with a 50 mm crack and an applied force of 100 N. The energy release rate has been calculated with a *p*-value of 6 and is normalised with respective peak value, see Tables 4 and 5. Since the

Table 4
Convergence study of normalised peak energy release rate, G, for $a = 50$ mm

p-Value	Interface		
	0°/0° (kJ/m^2)	90°/90° (kJ/m^2)	45°/45° (kJ/m^2)
2	1.58915	3.59486	9.32559
3	1.48501	3.44602	8.00741
4	1.48485	3.40212	7.80944
5	1.48607	3.39756	7.82885
6	1.48513	3.39591	7.76059

Table 5
Convergence study of average energy release rate, G, for $a = 50$ mm

p-Value	Interface		
	0°/0° (kJ/m^2)	90°/90° (kJ/m^2)	45°/45° (kJ/m^2)
2	1.48812	3.48003	5.60311
3	1.40267	3.30822	5.30476
4	1.39237	3.26569	5.24358
5	1.39238	3.25810	5.24088
6	1.39223	3.25601	5.23544

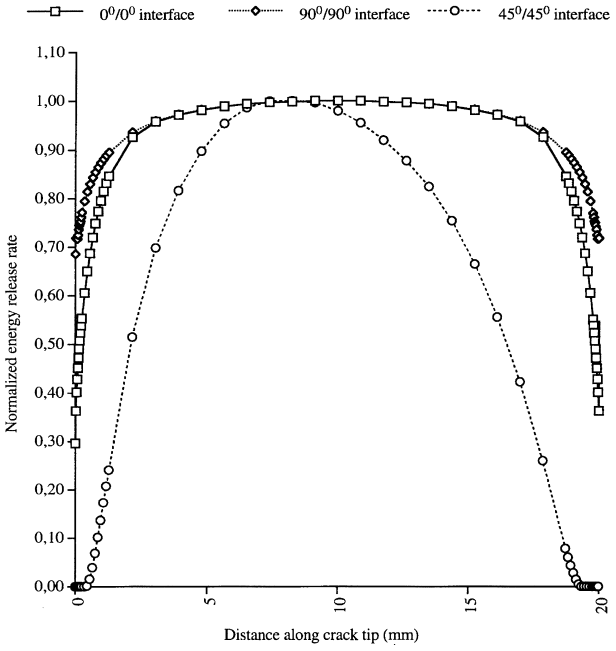

Fig. 13. G_I distribution for a DCB specimen with different interfaces.

layup of the specimens is symmetric with respect to the plane of the crack, only mode I energy release rate is globally possible. For the specimens with 0°/0° and 90°/90° interfaces the energy release rate is fairly constant in the interior of the specimens and approaches zero at the point where the crack tip intersects the free surface. This is due to the vertex singularity occurring at this point and has been described elsewhere [6].

The situation is more complicated for the specimens with a 45°/45° interface. On both sides of the specimens, close to the free surface, the crack surfaces will be in contact with each other. Since the FEM-model does not contain contact elements, the surfaces interpenetrated each other in the contact region and the energy release rate has been set to zero in that region. It has been reported, [10], that if contact elements are used the region of contact decreases and the energy release rate at the centre of the specimen increases slightly. The distribution of energy release rate is unsymmetrical because of the 45°/45° interface. It should be noted that the region of a fairly constant energy release rate is small in the case of a 45°/45° interface.

4.3. Subcritical crack growth

Since the energy release rate is not constant along the crack tip for any of the specimens, it can be anticipated that subcritical crack growth will occur where the energy release rate has a maximum. This will cause the crack to become curved, see Fig. 10, probably in such a way that the energy release rate becomes constant along the crack tip. Since the energy release rate is zero in any region of contact, the crack tip will have to become curved in such a way that the contact will disappear for the specimen with a 45°/45° interface. The angle the crack tip makes with the free surface has been calculated as −14° for the 0°/0° interface, 3° for the 90°/90° interface and −25° and +8° for the 45°/45° interface, depending on which surface is considered, by considering the vertex singularity at the surface [6]. A negative angle means that the crack is longer at the centre than at the surface of the specimen. Any subcritical crack growth would give a non-linear force-displacement curve which has been experimentally observed by De Kalbermatten [11]. In this investigation non-linear force-displacement curves were also observed for non-zero interfaces.

The curvature of the crack tip will cause the crack to be longer in the interior than what is observed on the surface of the specimen. The crack front curvature has previously been modelled and for certain layups found to be significant [7,9,10]. This curving of the crack front will make it difficult to know which crack length to use in data analysis, since the crack will be longer at the centre of the specimen than what is measured at the specimen edge. The results in Fig. 13 would suggest that the crack front would be most curved for the specimens with a 45°/45° interface and the least curved for the specimens with a 90°/90° interface.

4.4. Comparison STRIPE - beam model

4.4.1. Compliance

In Fig. 14 the measured compliance is compared with that calculated by the finite element method. For all three types of specimens the measured compliance is higher than the calculated one. There are several possible reasons for this. Deformation of the specimen holder and testing machine would result in an apparently softer specimen. Matrix cracking in 90° and ±45° plies would also result in a softer specimen. It is not probable that matrix cracking would occur in the specimens with a 0°/0° interface since all plies are 0° plies, which are not prone to matrix cracking. Geometrical non-linearity might also influence the compliance, although it is not clear in what way.

During experiments the crack length is measured on the surface of the specimen. But, it has been experimentally observed that the delamination front will be curved in such a way that the crack is longer in the interior of the specimen than on the surface, see Fig. 10. In Fig. 15 the crack length has been increased 2 mm and 4 mm for the specimens with 0°/0° and 45°/45° interfaces, respectively, in order to compensate for the curved crack front. The data fit the calculated compliance curves fairly well after that operation. The 90°/90° interface has the flattest energy release rate distribution, see Fig. 13, and also the best agreement with the measured compliance. This would suggest that the results from the numerical modelling describes the deformation of the specimens well.

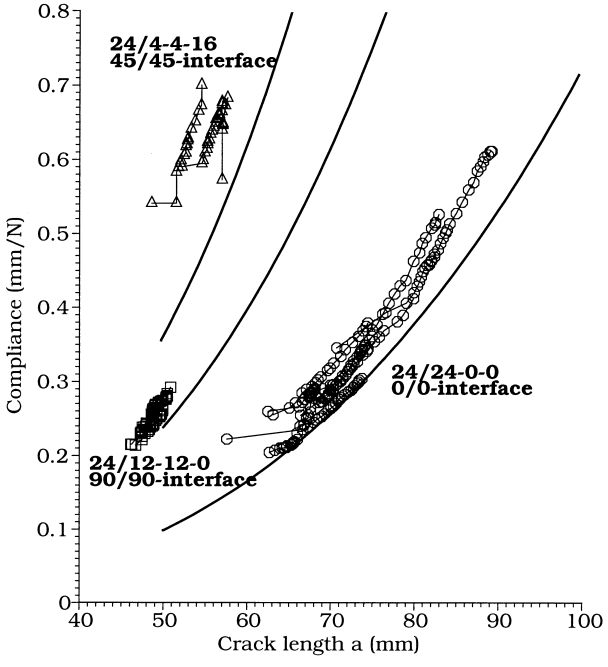

Fig. 14. Comparison between measured and FE compliance.

4.4.2. Different layups

In order to compare the energy release rate calculated with the simple beam theory, Eq. (1) with that obtained from the finite element method, crack opening values, δ, from the finite element method was substituted into Eq. (1). The energy release rate was also calculated with the beam model developed by Olsson [3]. In Olsson's model only geometry and ply material data were used as input. The model accounts for the rotation at the crack tip. The obtained energy release rates were compared to the average energy release rate given by the finite element method, see Fig. 16. For the 0°/0° and 90°/90° interfaces the model by Olsson is clearly closer to the FEM results than the simple beam model. The situation is reversed for the 45°/45° interface for which the crack surfaces are in contact close to the edges. If contact elements had been used in the analyses the result might have been different. The flatter the energy release rate distribution is for the interface, see Fig. 13, the more accurate the models are. For both beam models the error decreases as the crack length increases.

Krüger et. al. [21], have compared different 2-D nonlinear FE-analyses and found them yielding approximately 6% difference in results and when compared to the beam model a slightly higher difference. This 3-D analysis results in a smaller difference when compared to the beam model.

5. Implications for aircraft design

Since delamination growth is one of the more important failure mechanisms in aircraft composite structures, it is important to use a material system with high resistance to delamination growth. The DCB-specimen is useful to compare different material systems resistance to delamination growth during mode I loading.

For pure mode I loading in fatigue it does not seem possible to use delamination growth rate curves in the design process due to the very steep curves. The problem is rather a threshold problem. It should be noted that there is a large difference between the critical energy release rate for static loading and the approximate threshold value for fatigue loading. This leads to different load levels for delamination growth during static and fatigue loading. Given a delamination in a structure the ratio between delamination growth during static and fatigue loading is

$$\frac{G_{IC}}{G_{th}} = \left(\frac{K_{IC}}{K_{th}}\right)^2 = \left(\frac{\sigma_{static}}{\sigma_{fatigue}}\right)^2 \approx \frac{220}{80}$$

which give

$$\left(\frac{\sigma_{static}}{\sigma_{fatigue}}\right) \approx 1.7$$

where K_{IC} and K_{th} are stress-intensity factors for delamination growth at static and at threshold value and σ_{static} and $\sigma_{fatigue}$ is the stress in the structure which causes the energy release rate of a delamination in the structure to reach G_{Ic} and G_{th}, respectively. For mode II loading the situation is even worse with the ratio $\sigma_{static}/\sigma_{fatigue}$ being approximately 3 [26]. This should be compared with the ratio $\sigma_{DUL}/\sigma_{DLL}$ which often is 1.5,

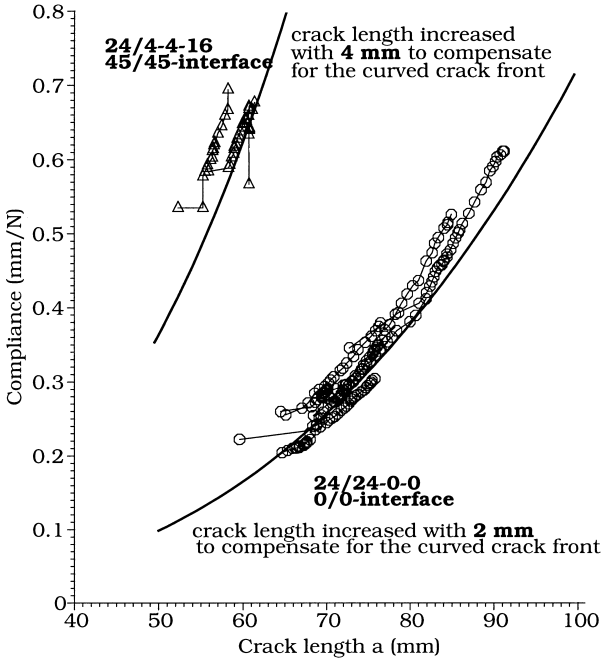

Fig. 15. Comparison between measured and FE compliance, adjustment of crack length.

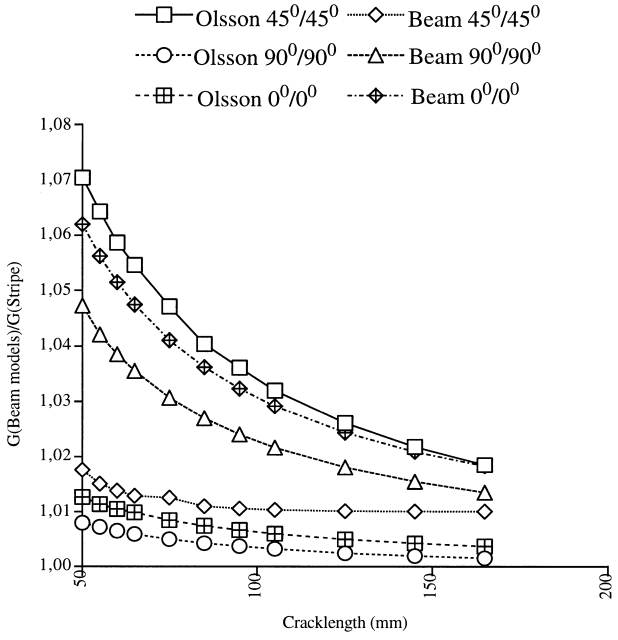

Fig. 16. Comparison between FE and different models.

where σ_{DUL} is the ultimate and σ_{DLL} is the limit static stress level to which composite structures are tested during certification. The limit stress level is also the maximum/minimum fatigue stress level to which the structure is subjected during fatigue loading. This means that a given delamination in a structure might not grow during static testing, but during fatigue testing it might grow. During certification of the AIRBUS A320 vertical fin, no delamination growth was detected during static loading. The following fatigue loading of the same component had to be interrupted due to large delamination growth. The delamination grew due to out-of-plane loads [22]. This demonstrates the importance of using the threshold value instead of the static value for delamination growth in design of composite structures. During both manufacture and service delamination damage is often discovered in aircraft composite structures. Normally, delamination growth is not allowed during operation of the aircraft. Therefore, it is necessary to determine if the damage requires any action to assume safe operation of the aircraft. Since the load levels required during certification for static and fatigue loading are different, it is necessary to determine if the critical energy release rate value is exceeded during static loading or if the threshold value is exceeded during fatigue loading for the delamination. If that is the case some type of repair could be required to assume safe operation of the aircraft.

6. Summary and conclusion

An extensive numerical and experimental investigation has been carried out for the DCB specimen. Data analysed with Berry's method and the corrected beam theory give similar results whereas data analysed with the simple beam theory results in higher energy release rates. The material systems IM7/8552 and HTA7/6376 have similar critical energy release rate whereas T300/914 has a significantly lower critical energy release rate. For non-zero interfaces intralaminar growth occurred through the 90 or 45 plies, giving raise to a hardening *R*-curve behaviour and a wavy appearance of the fracture surface. The plateau value of the R-curves was roughly four times that of the zero interface. Numerically predicted curved crack front for zero-interface could be verified experimentally. The cyclic delamination growth rates increased rapidly with increased ΔG. The energy release rate of the specimens have been calculated with *p*-version FEM, using converged solutions. Comparison between specimens with different layups showed that the specimens with a 90°/90° interface had the flattest energy release rate distribution along the crack tip and the specimens with a 45°/45° interface had the most uneven one. The calculated compliance compared well with the measured one after the curved crack front had been accounted for. Energy release rate calculated with a modified beam model has a smaller error than that calculated with the simple beam model.

Acknowledgements

The authors wish to express their thanks to the Swedish National Research Programme (NFFP2.39), the Defence Material Administration (HU4326) and to Saab AB who financed the work presented in this paper. The authors also want to thank Dr. Börje Andersson at the Aeronautical Research Institute of Sweden for his valuable help when performing their numerical calculations. We also greatly acknowledge Andrew Dolphin and Richard Sharp, British Aerospace Military Division, for valuble discussions and comments and for the permission to publish certain results.

References

[1] O'Brien TK, Martin RH. Round robin testing for mode I interlaminar fracture toughness of composite materials. J Compos Technol Res 1993;15(4):269–81.
[2] Hashemi S, Kinloch AJ, Williams JG. Proc R Soc Lond A 1990;427:451–9.
[3] Olsson R. A simplified improved beam analysis of the DCB-specimen. Compos Sci Technol 1992;43:329–38.
[4] Sun CT, Pandey RK. Improved method for calculating strain energy release rate based on beam theory. AIAA J 1994;32:184–9.
[5] Sun CT, Zheng S. Delamination characteristics of double-cantilever beam and end-notched flexure composite specimens. Compos Sci Technol 1996;56:451–9.
[6] Schön J, Andersson B. A theoretical study of the DCB and ENF test specimens. To be submitted to Journal of Applied Mechanics.
[7] Davidson BD, Schapery RA. Effect of finite width on deflection and energy release, rate on an orthotropic double cantilever specimen. J Compos Mater 1988;22:640–56.
[8] Davidson BD, Krüger R, König M. Effect of stacking sequence on energy release rate distributions in multidirectional DCB and ENF specimens. Eng Fract Mech 1996;55:557–69.
[9] Davidson BD. An analytical investigation of delamination front curvature in double cantilever beam specimens. J Compos Mater 1990;24:1124–37.
[10] Nilsson KE. On growth of crack fronts in the DCB-tes. Compos Eng 1993;3:527–46.
[11] Kalbermatten TDe, Jäggi R, Flüeler, Kausch HH, Davies P. Microfocus radiography studies during mode I interlaminar fracture tests on composites. J Mater Sci Lett 1992;11:543–6.
[12] Polaha JJ. Effect of interfacial ply orientation on the fracture toughness of a laminated composite, AIAA-94-1537-CP, pp. 1707–16.
[13] Polaha JJ, Davidson BD, Hudson RC, Pieracci A. Effect of mode ratio, ply orientation and precracking on the delamination toughness of a laminated composite. J Reinf Plast Compos 1996;15:141–73.
[14] Ireman T, et al. Damage propagation in composite structural elements-coupon experiments and analyses. Compos Struct 1996;36:209–20.

[15] Andersson B, Falck U, Babuska I, Von Petersdorff T. Reliable stress and fracture mechanics analysis of complex components using a h-*p* version of FEM. Int J Numer Meth Eng 1995;38:2135–63.
[16] European Structural Integrity Society–Polymer and Composite Task Force. Protocol for interlarninar fracture testing Nos. 1 and 2, March 1992.
[17] Standard test method for Mode 1 interlaminar fracture toughness of unidirectional fiber-reinforced polymer matrix composites. American Society For Testing and Materials, D 5528 - 94a.
[18] Granstam P. Fractographical examination of DCB tested carbon fibre composite samples. A Saab/BAe collaboration, CSM-T5447, 1996.
[19] Wilkins DJ, Eisenman JR, Camin RA, Margolis WS, Benson RA.Characterizing delamination growth in graphite-epoxy. Damage in composite materials, ASTM STP 775. American Society for Testing and Materials, 1982. p. 168–83.
[20] Chai H. The characterisation of Mode I delamination failure in non-woven, multidirectional laminates. Composites 1984;15:277–90.
[21] Krüger R, König M, Schneider T. Computation of local energy release rates along straight and curved delamination fronts of unidirectionally laminated DCB and ENF-specimens. In: Proceedings of the 34th AIAA/ASME/ASCE/AHS/ASC Structures, Structural Dynamics and Material Conference, April 1993, p. 1332–42.
[22] Laméris L. The use of load enhancement factor in the certification of composite aircraft structures. National Aerospace Laboratory the Netherlands, NLR TP 90068U.
[23] Prinz R, Gädke M. Characterisation of interlaminar mode I and mode II fracture in CFRP laminates. In: Proc. of Inter. Conf. on Spacecraft Structures and Mechanical Testing. ESA SP-321, 1991. p. 97–102.
[24] Hojo RM, Ochiai S, Gustavson CL, Tanaka K. Effect of matrix resin on delamination fatigue crack growth in CFRP laminates. Eng Fract Mech 1994;49:35–47.
[25] Martin RH, Murri GB. Characterization of mode I and mode II delamination growth and thresholds in AS4/PEEK composites. ASTM STP 1990; 1059: 251–70.
[26] Schön J, Nyman T, Blom A, Ansell, H. A numerical and experimental investgation of a composite ENF-specimen. Submitted to Engineering Fracture Mechanics.